Preprint Title	Organic Thermally Activated Delayed Fluorescence Material with Strained Benzoguanidine Donor
Authors	Alexander C. Brannan, Elvie F. P. Beaumont, Nguyen L. Phuoc, George F. S. Whitehead, Mikko Linnolahti and Alexander S. Romanov
Publication Date	28 Juni 2023
Article Type	Full Research Paper
Supporting Information File 1	Supporting Information.docx; 2.2 MB
Supporting Information File 2	lar9.cif; 1.5 MB
ORCID® iDs	Alexander C. Brannan - https://orcid.org/0000-0002-9640-2594; Elvie F. P. Beaumont - https://orcid.org/0009-0002-8553-306X; George F. S. Whitehead - https://orcid.org/0000-0003-1949-4250; Mikko Linnolahti - https://orcid.org/0000-0003-0056-2698; Alexander S. Romanov - https://orcid.org/0000-0003-2617-6402

Organic Thermally Activated Delayed Fluorescence Material with Strained Benzoguanidine Donor

Alexander C. Brannan[1], Elvie F. P. Beaumont[1], Nguyen Le Phuoc[2], George F. S. Whitehead[1], Mikko Linnolahti*[2] and Alexander S. Romanov*[1]

Address: [1]Department of Chemistry, The University of Manchester, Manchester, United Kingdom, [2]Department of Chemistry, University of Eastern Finland, Joensuu, Finland

Email: Alexander S. Romanov – alexander.romanov@manchester.ac.uk
Mikko Linnolahti - mikko.linnolahti@uef.fi
* Corresponding author

Abstract

Organic thermally activated delayed fluorescence materials (TADF) have been widely investigated due to their impressive electronic properties and applied potential for the third generation of organic light-emitting diodes (OLED). We present organic TADF material (4BGIPN) based on the strained benzoguanidine donor and compare it with the benchmark carbazole-based material (4CzIPN). Extended π-conjugation in 4BzIPN material results in yellow luminescence at 525 nm with a fast radiative rate of 1.15×10^{-6} s^{-1} and photoluminescence quantum yield of 46% in methylcyclohexane solution. Such a nitrogen-rich 4BGIPN material has a significantly stabilized highest occupied molecular orbital (HOMO) at –6.4 eV while the lowest unoccupied molecular orbital (LUMO) at -4.0 eV, indicating potential suitability for application as the electron transport layer or TADF class III emitter in OLEDs.

Keywords

Organic; TADF; yellow; guanidine; photoluminescence

Introduction

Thermally activated delayed fluorescence (TADF) is a photoluminescence mechanism where excitons undergo thermally-assisted reverse-intersystem crossing from an excited triplet state to a higher-lying in energy singlet state to emit delayed fluorescence.[1–3] Organic TADF emitters have gained substantial attention in recent years for their prospective application in organic light-emitting diodes (OLEDs), photocatalysis, bioimaging and sensors.[4–6] The ability to harvest both singlet and triplet excitons enabled organic TADF emitters to compete with classic phosphorescent emitters that employ scarce metals such as iridium and platinum.[7–9] Since its first report in 2012 by Uoyama et al., 1,2,3,5-tetrakis(carbazol-9-yl)-4,6-dicyanobenzene (4CzIPN) has been a benchmark TADF emitter due to its high quantum yields and excellent performance in OLED devices.[1] 4CzIPN is a donor-acceptor type system where carbazole donor ligands are bound to the benzonitrile acceptor core moiety. In this work we have substituted the carbazole donors with 5*H*-benzo[*d*]benzo[4,5]imidazo[1,2-*a*]imidazole (benzoguanidine) ligands, see Scheme 1, to give **4BGIPN**. Benzoguanidine has an extended pi-conjugation compared with carbazole and is more nitrogen-rich (three N-atoms vs one in carbazole). Thompson et al., recently reported a series of carbene-metal-amide (CMA) (metal = Cu, Ag, Au) emitters employing a benzoguanidine ligand.[10] The extended pi-conjugation of benzogunaidine induced a larger hole−electron separation resulting in a smaller energy gap between the excited singlet and triplet states (S_1 and T_1) and ΔE_{ST} resulting in faster radiative rates. This study aimed to synthesize and explore the luminescent properties of the 4BGIPN material containing a rigid benzoguanidine ligand in its molecular structure.

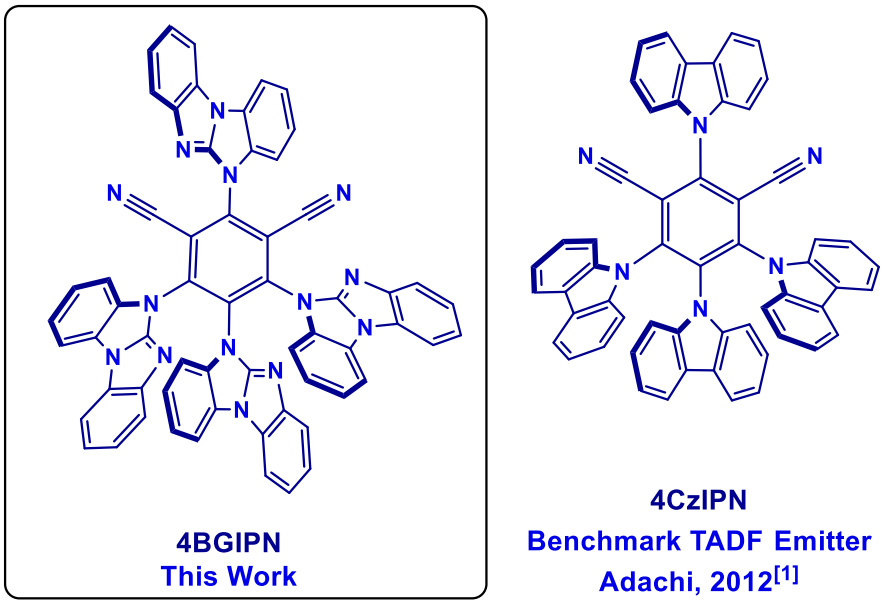

Chart 1. The molecular structures of the title compound **4BGIPN** and the benchmark TADF emitter 4CzIPN.

Results and Discussion

Synthesis and Structure.

4BGIPN was prepared in 70% yield by aromatic nucleophilic substitution reaction from 2,4,5,6-tetrafluoroisophthalonitrile and 5*H*-benzo[*d*]benzo[4,5]imidazo[1,2-*a*]imidazole (benzoguanidine) after deprotonation the later with sodium hydride base. The compound shows poor solubility in most common organic solvents with moderate solubility in dichloromethane, 1,2-dichlorobenzene and dimethylsulfoxide (DMSO). Compound **4BGIPN** was characterized by ^{1}H and ^{13}C NMR and high-resolution mass spectrometry. Proton NMR shows a complicated set of overlapping multiplets which is likely associated with multiple rotamers present in the solution experiencing a constant dynamic process (twisting and tilting of the benzoguanidine donor moieties). The decomposition temperature (T_d, corresponds to 5% weight loss) was measured with thermogravimetric analysis (TGA) indicating excellent thermal stability for **4BGIPN** with T_d = 425°C, which is similar to a benchmark material 4CzIPN having T_d in the range 402–449°C (T_d range dependent on the type of the 4CzIPN polymorph).[11,12]

Single crystals for X-ray diffraction study were obtained by slow layer diffusion of hexanes into dichloromethane solution for **4BGIPN** at room temperature (Figure 1). The title compound crystallizes with two independent molecules in the unit cell of the chiral space group *P2₁*. Two independent molecules of **4BGIPN** are related by a pseudo glide plane that do not completely align when superimposed through a glide operation. There is no evidence for systematic absences relating to the presence of a glide plane in the data supporting the refinement in the chiral *P2₁* space group. The structure was refined as a two-component inversion twin; the crystal structure as a whole is a racemic mixture of both orientations. The $C_{benzene}$–$N_{benzoguanidine}$ bond length varies within the error of the experiment from 1.402(5) to 1.420(5), giving an average of 1.407(13) Å for **4BGIPN**, which is closely similar to 1.405(8) Å reported for the benchmark 4CZIPN compound. Unlike carbazole, the benzoguanidine ligand lacks C_2 rotational symmetry, thus enabling the benzoguanidine ligands to project above and below the plane of the central benzene ring. In both molecules in the asymmetric unit, the benzoguanidine moiety bound to the benzene carbon neighboring two nitrile groups, is orientated in the opposing projection about the plane of the benzene ring to the remaining benzoguanidine moieties. Compound **4BGIPN** possesses a twisted orientation between the donor (benzoguanidine) and acceptor (benzonitrile) ligands (Figure 1) due to steric hindrance imposed by benzoguanidine ligands and reflected by the torsion angle (α) laying in the range of 42.5(2)–64.3(2)º. We compare it with more narrow torsion angle range of 55.1(2)–60.2(2)º for 4CzIPN thus indicating that various carbazole donor ligands possess a very similar twist

orientation.[12] The donor-acceptor twist angle has been demonstrated to be one of the key structural parameters enabling fast radiative rates for purely organic TADF materials since it's directly related with the overlap integral between HOMO and LUMO orbitals and influences the energy differences between first singlet and triplet excited states.[13] Therefore, we expect a marked difference in the photophysical properties for 4BGIPN, *vide infra*.

Analysis of the intermolecular interactions revealed that 4BGIPN molecules experience a face to face intermolecular π-π stacking interactions between the benzoguanidine moieties similar to 4CzIPN (reported by Etherington et al.).[12] The average interplanar distance for close neighbor benzoguanidine moieties in **4BGIPN** is 3.322(3) Å, which is significantly shorter (0.4 Å) than the 3.74(3) Å average distance between nearest neighbor carbazole ligands in 4CzIPN, indicative for much stronger intermolecular interactions.

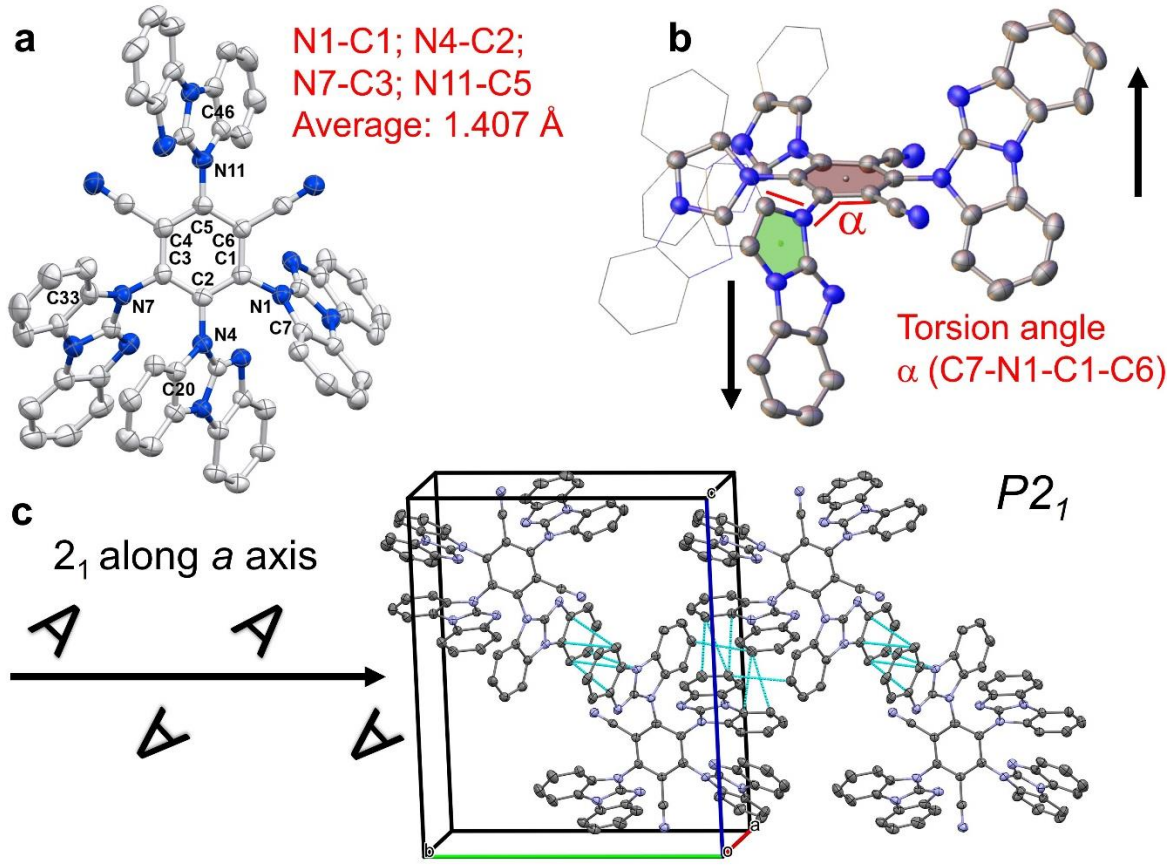

Figure 1. Crystal structure for compound **4BGIPN** (**a**, top view and **b**, side view) where black arrows show opposite orientation of the benzoguanidine moieties around central benzene ring. Representative example for the torsion angle α is shown in red; (**c**) packing diagram with key geometrical parameters and intermolecular contacts shown as a cyan dashed line. Ellipsoids are shown at the 50% level where hydrogen atoms are omitted for clarity.

Cyclic voltammetry was used to analyze the redox behavior of the **4BGIPN** in THF solution containing [n-Bu_4N]PF_6 as supporting electrolyte (Figure 2, Table 1). The reduction wave has a quasi-reversible character with the $E_{1/2}$ at –1.50 V, which is 260 mV shifted to higher potential when compared with 4CzIPN (–1.76 V) under similar conditions in THF.[14] Compounds **4BGIPN** and 4CzIPN experience reduction process at the benzonitrile core (see, the LUMO isosurface in Figure 5, *vide infra*). Therefore, the higher reduction potential for **4BGIPN** suggests that the benzonitrile core has lower electron density, which is likely associated with extended π-conjugation and two additional electron withdrawing aza-type nitrogen atoms in the benzoguanidine moieties. This explains *ca.* 0.2 eV more stabilized LUMO energy level for compound **4BGIPN** compared with 4CzIPN. Both 4CzIPN and **4BGIPN** exhibit an irreversible oxidation wave observed at +1.25 V for **4BGIPN** in THF and +0.94 V for 4CzIPN in MeCN.[14] A higher oxidation potential (E_p) for **4BGIPN** compared with the 4CzIPN corroborates with the electron deficient nature of the benzoguanidine moiety thus making it harder to oxidize compared with more electron rich carbazole moiety. This results in stabilization of the HOMO energy level at –6.4 eV for **4BGIPN**. Significant stabilization for both HOMO and LUMO energy levels indicates the potential suitability of **4BGIPN** material for application not only as emitter in emitting layer but also as an electron transport layer in the fabrication of OLEDs.

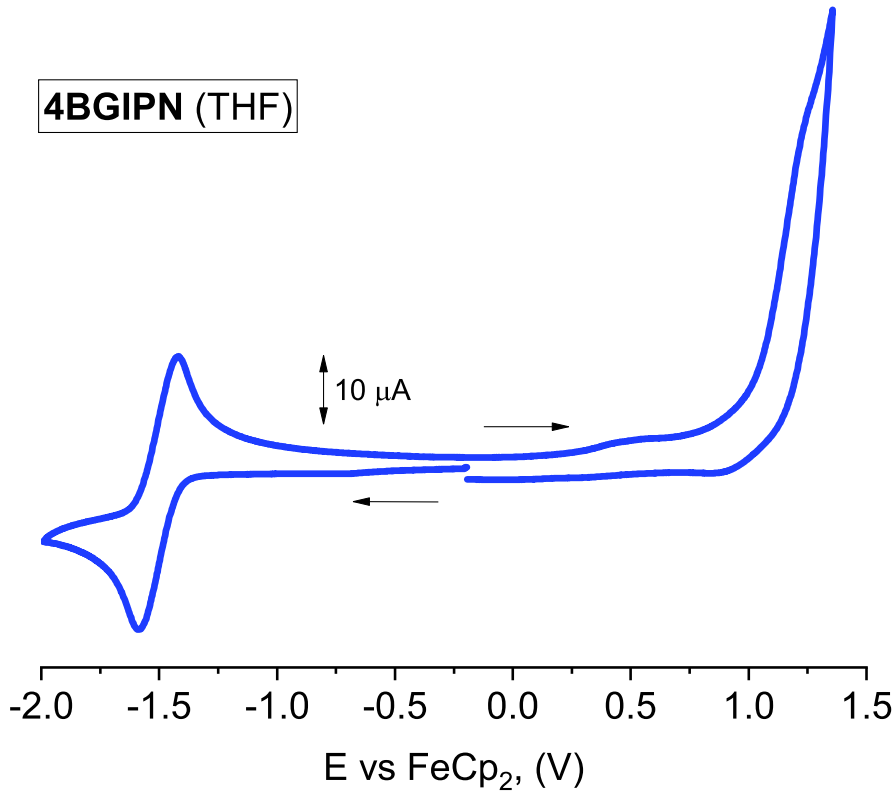

Figure 2: Full range cyclic voltammogram for **4BGIPN**. Recorded using a glassy carbon electrode in THF solution (1.4 mM) with [n-Bu_4N]PF_6 as supporting electrolyte (0.13 M), scan rate 0.1 Vs^{-1}.

Table 1. Formal electrode potentials (peak position E_p for irreversible and $E_{1/2}$ for quasi-reversible processes (*), *V*, *vs*. $FeCp_2$), onset potentials (*E*, *V*, *vs*. $FeCp_2$), peak-to-peak separation in parentheses for quasi-reversible processes (ΔE_p in mV), E_{HOMO}/E_{LUMO} (*e*V) and band gap values (ΔE, *e*V) for the redox changes exhibited by **4BGIPN**.[a]

Complex	Reduction		E_{LUMO}	Oxidation		E_{HOMO}	ΔE
	E_{1st}	$E_{onset\ red}$	eV	E_{1st}	$E_{onset\ ox}$	eV	eV
4BGIPN	-1.50 (167)	-1.41	-3.98	+1.25	+1.01	-6.40	2.42

In THF solution, recorded using a glassy carbon electrode, concentration 1.4 m*M*, supporting electrolyte [^{n}Bu_4N][PF_6] (0.13 *M*), measured at 0.1 V s^{-1}. [b]In THF solution, recorded using a glassy carbon electrode, concentration 1.4 m*M*, supporting electrolyte [^{n}Bu_4N][PF_6] (0.13 *M*), measured at 0.1 V s^{-1}. $E_{HOMO} = -(E_{onset\ ox\ Fc/Fc+} + 5.39)$ *e*V; $E_{LUMO} = -(E_{onset\ red\ Fc/Fc+} + 5.39)$ eV.[16]

Photophysical Properties and Theoretical Considerations

UV-vis and photoluminescence (PL) spectra for **4BGIPN** are shown in Figures 3 and 4 while data in various media is collected in Tables 2 and 3, respectively. UV-vis absorption spectra of 4BGIPN show a strong π–π* intraligand transition (IL, benzoguanidine) at 290 nm with ε = 42000 $M^{-1}cm^{-1}$. Unlike 4CzIPN, we do not observe any vibronically resolved carbazole absorption peaks which are commonly present at 325 nm.[15] Similar to 4CzIPN,[14,15] the UV-vis profile has two broad regions: localized charge transfer (^{lo}CT) over 320–380 nm region with ε up to 14000 M^{-1} cm^{-1} and a delocalized charge transfer (^{de}CT) broad shoulder over the region ca. 380–460 nm with ε up to 1900 M^{-1} cm^{-1} (Table 2). Both ^{lo}CT and ^{de}CT bands are observed for the benchmark material 4CzIPN[17] while originating from HOMO to LUMO transition in line with the theoretical calculations (Table S1 and S3). All CT bands experience a very weak solvatochromic effect with increasing solvent polarity from cyclohexane to dichloromethane. This indicates only minor change of the transition dipole moment upon vertical excitation from S_0 (6.4 D) to S_1 (7.2 D) excited states according to the TD-DFT theoretical calculations (Table S2).

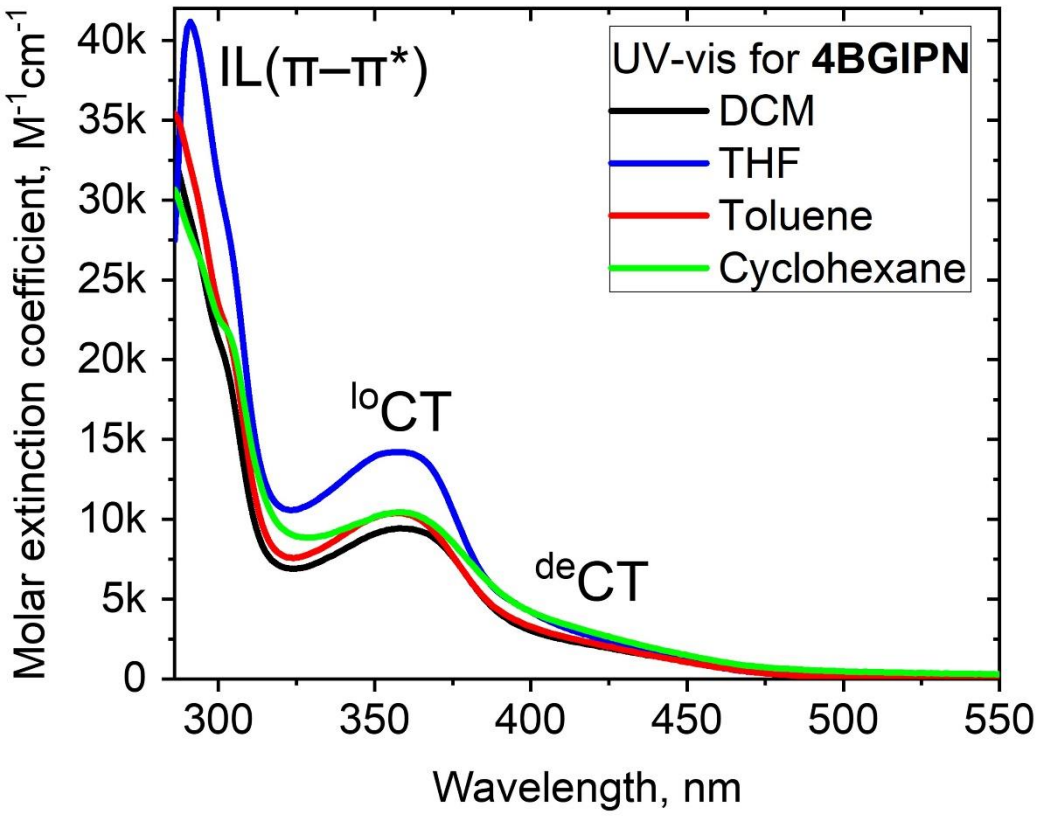

Figure 3: UV-vis absorption spectra for compound **4BGIPN** in various solvents.

Table 2. UV-vis data for compounds **4BGIPN** and 4CzIPN[14,15] in various solvents.

	λ_{abs} [nm], (10^3 ε/M^{-1} cm^{-1})			
	DCM	THF	Toluene	Cyclohexane
4BGIPN	436 sh (1.5) 358 (9.5)	435 sh (1.8) 357 (14.2)	439 sh (1.4) 358 (10.4)	439 sh (1.9) 358 (10.5)
4CzIPN	448 (7)[14] 378[15]	438 (8)[14] –	441 (6)[14] 375[15]	N/A

The photoluminescence (PL) characteristics of **4BGIPN** have been studied in methylcyclohexane solution (MCH, concentration 3.2×10^{-5} M) and Zeonex polymer films (0.1% concentration by weight) at 298K and 77K, which is shown in Figure 4 with data collected in Table 3. Compound **4BGIPN** exhibits a featureless yellow CT-type luminescence with λ_{max} = 525 nm that is 44 and 25 nm red-shifted compared to 4CzIPN (λ_{max} = 481 and 500 nm in Zeonex and MCH, respectively).[12] The solution photoluminescent quantum yield

(PLQY) of **4BGIPN** is 46% under inert atmosphere and decreases down to 18% in aerated MCH solution. The reduction in quantum yield on exposure to oxygen is due to quenching of the triplet excited states indicating a TADF luminescence mechanism. PLQY in Zeonex films is 39% in air, which is lower than the PLQY of 87% reported for 4CzIPN.[14]

The two-component excited state lifetime with prompt and delayed fluorescence is characteristic for the TADF-type luminescence.[1] The excited state lifetime of **4BGIPN** has a biexponential decay with a prompt fluorescence $\boldsymbol{\tau}_p$ = 13 ns and a delayed fluorescence $\boldsymbol{\tau}_d$ = 955 ns components in MCH solution. Zeonex films of **4BGIPN** exhibit a similar prompt $\boldsymbol{\tau}_p$ = 12 ns, but an almost three-fold longer delayed fluorescence $\boldsymbol{\tau}_d$ = 2.4 μs when compared to MCH solution. The archetype material 4CzIPN possesses a similar prompt fluorescence component of 8 ns, whereas a delayed component is nearly ten-times longer, 8.9 and 8.8 μs, in MCH and Zeonex films, respectively.[12] These measurements correlate well with lower PLQY values for **4BGIPN** compared with 4CzIPN, thus indicating that the use of a larger benzoguanidine donor ligand may open more nonradiative processes. This is reflected in the larger distribution in the torsion angles for **4BGIPN** compound compared with 4CzIPN, *vide supra*.

We collected PL characteristics for **4BGIPN** at 77K to further support the assignment of the TADF mechanism. The emission profiles experienced minor narrowing upon cooling to 77K, while the PL profile remained broad and featureless (Figure 4e and f). Notably, a frozen MCH glass exhibits a new vibronically-resolved component at 422 nm, together with a broad CT profile. The excited state lifetime of the broad CT-component has a multiexponential decay with averaged lifetimes of 421 μs in MCH-glass and 540 μs in Zeonex films, which we assigned as phosphorescence from a ^{3}CT state. A more than 100-fold increase in radiative lifetime on cooling to 77K is characteristic for the organic TADF emitters.[1] The resolved high energy PL-component at 422 nm has a lifetime of 4.2 ms, which we assign to a phosphorescence from a higher lying ^{3}LE state localized on a donor-benzoguanidine moiety. Excitation spectra of the broad and resolved bands for 4BGIPN in MCH glass at 77K (Figure 4b) follow a mirror image rule when compared with emission spectra showing both broad and resolved components, thus supporting the assignments of the ^{3}CT and ^{3}LE(donor) excited states.

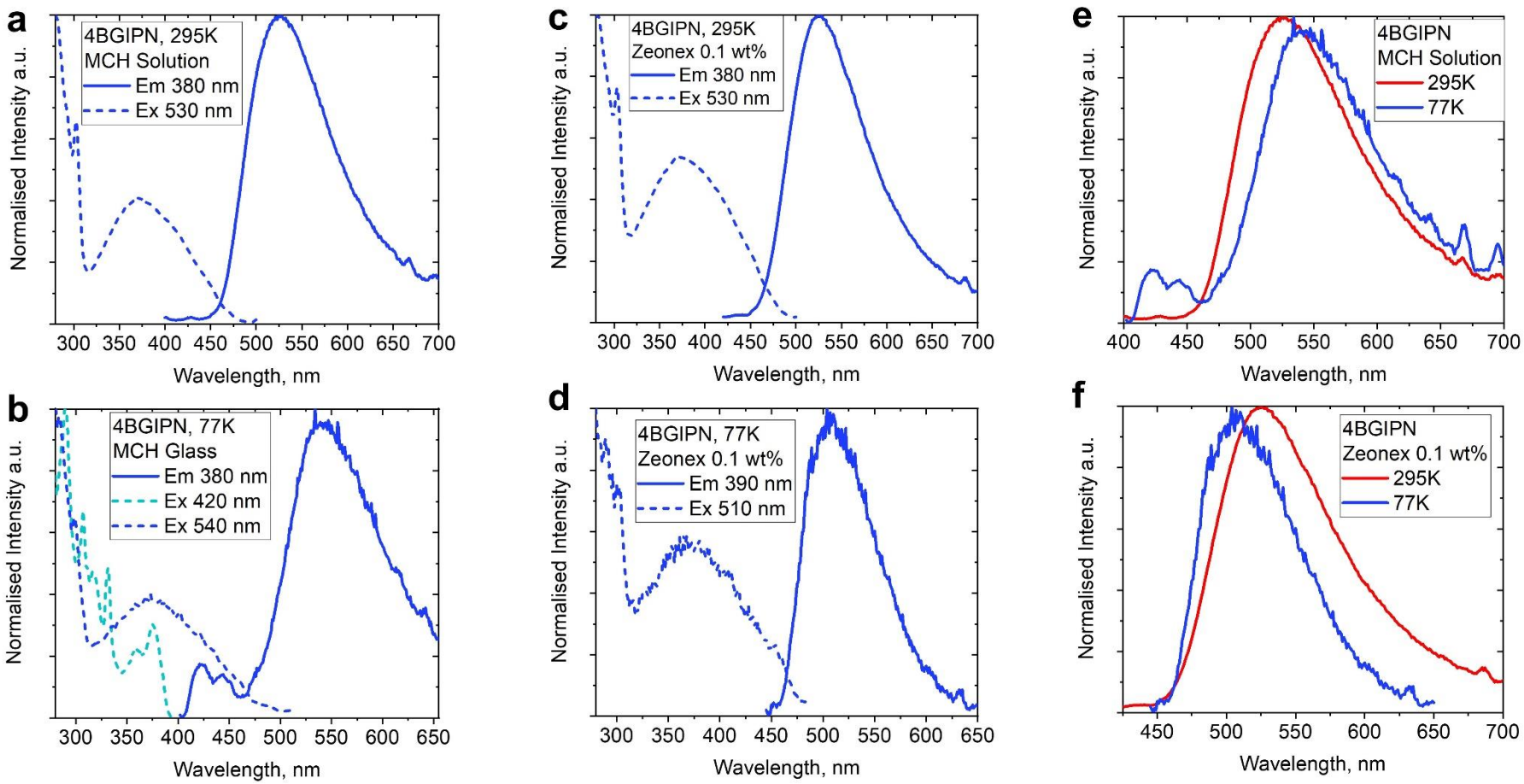

Figure 4: Photoluminescence spectra for 4BGIPN in a) MCH solutions and b) Zeonex 0.1 wt% films at 295K and 77K with emission and excitation wavelengths given.

Table 3. Photophysical properties of **4BGIPN** in various media at 295 and 77K.

	λ_{em} (nm)	τ (ns)	Φ (%)[a]	k_r (10^6 s^{-1})[b]	k_{nr} (10^6 s^{-1})[c]	^{1}CT/^{3}CT/^{3}LE (eV)[d]	λ_{em} (nm, 77K)	τ (μs, 77K)
Methylcyclohexane (MCH) solution								
4BGIPN	525	12.6 (59%) 955 (41%)	46 (N_2) (18 air)	1.15	1.35	2.68/2.61/3.04	421 (^{3}LE); 539 (^{3}CT)	4200 7.84 (52%) 146 (14%) 1166 (34%)
0.1 wt% Zeonex matrix								
4BGIPN	525	11.9 (43%) 2329 (57%)	39	0.29	0.46	2.67/2.60/–	506	3.98 (52%) 101 (14%) 1541 (34%)

[a] absolute quantum yields determined using an integrating sphere; [b] radiative rate constant $k_r = \Phi/\tau$; [c] nonradiative constant $k_{nr} = (1 - \Phi)/\tau$. In case of two-component lifetime τ an average was used: $\tau_{av} = (B_1/(B_1 + B_2))\tau_1 + (B_2/(B_1 + B_2))\tau_2$, where B_1 and B_2 are the relative amplitudes for τ_1 and τ_2, respectively; [d] CT/LE energies based on the onset values of the emission spectra blue edges at 77 K and 295 K.

The charge transfer singlet (^{1}CT), triplet (^{3}CT) and local excited triplet (^{3}LE) state energies were estimated from the onset values of the blue emission edge of the PL spectra at 295K for ^{1}CT and 77K, respectively (Figure 4 and Table 3). The energy of ^{3}LE triplet state is 3.04 eV, whereas the energy of the ^{3}CT state is 2.61 eV and 0.07 eV lower compared to the energy of the singlet ^{1}CT state of 2.68 eV (Figure 5). Therefore, we ascribe compound **4BGIPN** to the class III TADF material where the ^{3}LE is higher in energy than the manifold of the CT states as shown on Figure 5.[18] The energy difference between singlet and triplet excited states is +0.07 eV for $\Delta E_{1CT\text{-}3CT}$ and –0.36 eV for $\Delta E_{1CT\text{-}3LE}$. Such small energy ΔE_{ST} values further support the assignment of the TADF mechanism for the compound **4BGIPN**. Theoretical results (Table S3 and S4) support our experimental observations, suggesting that low energy triplet states (T_1, T_2 and T_3) possess a mixed CT/LE character with energy difference up to 0.2 eV to the first singlet state S_1. At the same time, Class III TADF ($E_{3LE} > E_{CT}$)[19] and class II TADF materials ($E_{3LE} \approx E_{CT}$)[20] are reported to have shorter excited state lifetime compared with class I TADF materials, for instance 4CzIPN ($\Delta E_{1CT\text{-}3LE}$ = +0.09 eV[12]). Short microsecond excited state lifetime for **4BGIPN** (regardless of somewhat lower PLQY) is in line with those reported for other TADF class III systems.[19]

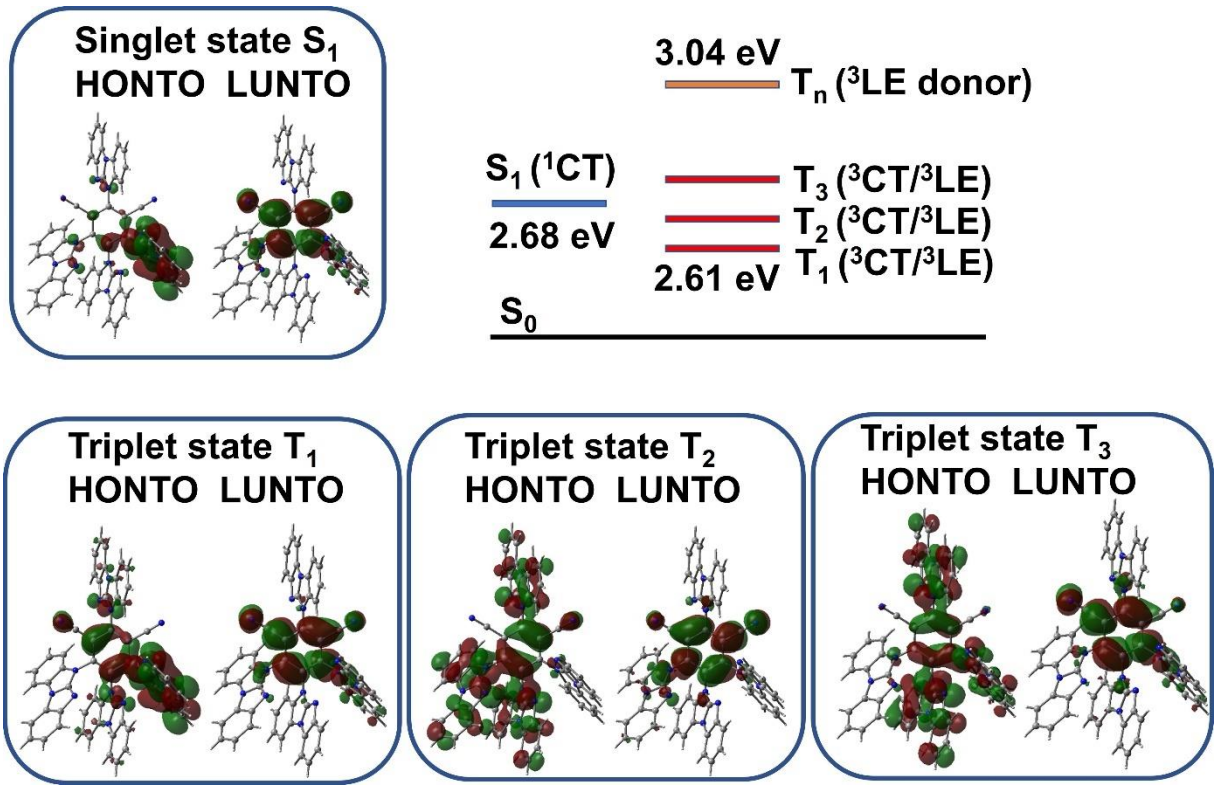

Figure 5. The energy state diagram and the natural transition orbitals HONTO and LUNTO for compound **4BGIPN** in excited **S_1**, **T_1**, **T_2** and **T_3** states calculated from the crystal S_0 geometry.

Conclusion

We have synthesized and characterized a donor-acceptor type thermally activated delayed fluorescent emitter **4BGIPN** with four terminal benzoguanidine donor moieties surrounding the benzonitrile acceptor core. The twisted structure of the **4BGIPN** ensures that the donor groups accommodate the highest occupied molecular orbital (HOMO) while the acceptor 4,6-dicyanobenzene moiety contains the lowest unoccupied molecular orbital (LUMO) and is supported by the TD-DFT calculations. Unlike the 4CzIPN compound, the **4BGIPN** emitter possesses parallel and antiparallel orientation of the benzoguanidine donors with respect to each other due to lack of C_2 rotational symmetry and extended π-conjugation compared to carbazole donor in 4CzIPN. A comparison of the electronic parameters between benchmark 4CzIPN and new **4BGIPN** materials revealed that benzoguanidine acts as a weaker donor ligand compared with carbazole, resulting in greater stabilization of the HOMO energy level down to –6.4 eV rather than LUMO. The significant stabilization of both HOMO and LUMO energy levels, along with multiple electron-withdrawing aza-nitrogen atoms in the structure of **4BGIPN**, suggests its potential suitability as an electron transport layer in OLED (organic light-emitting diode) devices. Variable temperature photoluminescence studies revealed that **4BGIPN** corresponds to class III TADF system ($E_{3LE} > E_{1CT}$), while having a small energy difference between singlet and triplet charge transfer excited states +0.07 eV for $\Delta E_{1CT\text{-}3CT}$. Theoretical calculations support that the first three triplet excited states possess a mixed CT/LE character while benzoguanidine triplet ^{3}LE state is much higher in energy than the singlet ^{1}CT state. The high quantum yields of up to 46% indicate that the yellow-green **4BGIPN** emitter shows promise as a platform for developing bright TADF class III materials. The sub-microsecond excited state lifetime for TADF class III materials, and future 4BGIPN analogs in particular, would be an important characteristic for fabricating TADF OLED devices with improved operating stability.

Experimental

General Considerations.

All reactions were performed under a N_2 atmosphere. Solvents were dried as required. Sodium hydride was washed from mineral oil with diethyl ether and dried prior to use. 5*H*-benzo[*d*]benzo[4,5]imidazo[1,2-*a*]imidazole or (benzoguanidine) was obtained according to the literature protocol[10] while 2,4,5,6-tetrafluoroisophthalonitrile was purchased from Fluorochem Ltd. and used as received. ^{1}H and $^{13}C\{^{1}H\}$ NMR spectra were recorded using a Bruker AVIII HD 500 MHz NMR spectrometer. ^{1}H NMR spectra (500.19 MHz) and $^{13}C\{^{1}H\}$ (125.79 MHz) were referenced to dichloromethane-d_2 at δ 5.32 (^{13}C, δ 53.84). All electrochemical experiments were performed using an Autolab PGSTAT 302N computer-controlled potentiostat. Cyclic voltammetry (CV) was performed using a three-electrode configuration consisting of a glassy carbon macrodisk working electrode (GCE) (diameter of 3 mm; BASi, Indiana, U.S.A.) combined with a Pt wire counter electrode (99.99%; GoodFellow, Cambridge, U.K.) and an Ag wire pseudoreference electrode (99.99%; GoodFellow, Cambridge, U.K.). The GCE was polished between experiments using alumina slurry (0.3 μm), rinsed in distilled water and subjected to brief sonication to remove any adhering alumina microparticles. The metal electrodes were then dried in an oven at 100 °C to remove residual traces of water, the GCE was left to air dry and residual traces of water were removed under vacuum. The Ag wire pseudoreference electrodes were calibrated to the ferrocene/ferrocenium couple in THF at the end of each run to allow for any drift in potential, following IUPAC recommendations.[16] All electrochemical measurements were performed at ambient temperatures under an inert N_2 atmosphere in THF containing the complex under study (0.14 mM) and the supporting electrolyte [*n*-Bu_4N][PF_6] (0.13 mM). Data were recorded with Autolab NOVA software (v. 1.11). Thermogravimetric analysis was performed by the Microanalysis Laboratory at the University of Manchester. Mass spectrometry data were obtained by the Mass Spectrometry Laboratory at the University of Manchester.

Synthesis of 4BGIPN. 5*H*-benzo[*d*]benzo[4,5]imidazo[1,2-*a*]imidazole (benzoguanidine)[10] (700 mg, 3.38 mmol) was added to a suspension of NaH (81.0 mg, 3.38 mmol) in anhydrous DMF (40 ml) at 0°C under a stream of N_2. The reaction mixture was stirred for 1 h at room temperature. 2,4,5,6-tetrafluoroisophthalonitrile (135 mg, 676 μmol) was added to the reaction mixture under N_2. The reaction mixture was heated to 140°C and left to stir overnight. The reaction mixture was dried under vacuum to remove DMF. The crude product was extracted with DCM and washed with water. The organic phase was collected and dried with $MgSO_4$,

filtered and concentrated under vacuo. The product was further purified by column chromatography (ethyl acetate:hexane 1:4) to give the pure product as a yellow powder in 70% yield (450 mg, 474 μmol). Single crystals suitable for X-ray diffraction were grown by layering a concentrated solution in DCM with hexane which was left for slow evaporation. ^{1}H NMR (400 MHz, DMSO-d_6) δ 8.54 – 6.81 (m, 31H), 6.44–6.25 (m, 1H). ^{13}C{^{1}H} NMR (126 MHz, CD_2Cl_2) δ 151.17, 149.67, 146.84, 146.65, 146.27, 142.44, 142.29, 142.01, 134.45, 133.78, 133.00, 132.63, 131.91, 130.98, 128.91, 128.50, 127.82, 126.78, 126.58, 126.41, 126.24, 125.84, 124.85, 124.51, 124.39, 124.22, 124.11, 124.01, 123.82, 123.71, 123.53, 123.38, 123.30, 123.23, 122.97, 122.76, 121.99, 121.91, 121.61, 121.41, 121.28, 120.01, 119.91, 119.68, 119.43, 119.16, 117.13, 112.60, 112.41, 112.06, 112.00, 111.69, 111.33, 111.21, 111.11, 110.88, 110.82, 110.74, 110.44, 110.17 ppm.

HRMS $C_{60}H_{32}N_{14}$ theoretical $[M+Na]^+$ = 971.2827, HRMS (ESI): = 971.2854.

X-Ray Crystallography.

Crystals suitable for X-ray diffraction study were obtained by slow layer diffusion of hexanes/petroleum ether into dichloromethane solution for **4BGIPN** at room temperature. Crystals were mounted in oil on a MiTeGen loop and fixed on the diffractometer in a cold nitrogen stream. Data were collected using dual wavelength Rigaku FR-X rotating anode diffractometer using CuKα (λ = 1.54146 Å) radiation, equipped with an AFC-11 4-circle kappa goniometer, VariMAX^{TM} microfocus optics, a Hypix-6000HE detector and an Oxford Cryosystems 800 plus nitrogen flow gas system, at a temperature of 100K. Data were collected and reduced using CrysAlisPro v42.[21,22] Absorption correction was performed using empirical methods (SCALE3 ABSPACK) based upon symmetry-equivalent reflections combined with measurements at different azimuthal angles.

For the final refinement, the contribution of severely disordered CH_2Cl_2 molecules in the crystals **4BGIPN** was accounted for by applying a solvent void mask calculated using BYPASS, implemented through Olex2.[23] Structures were solved by direct method/intrinsic phasing and refined by the full-matrix least-squares against F^2. All non-hydrogen atoms were refined with anisotropic atomic displacement parameters. All hydrogen atoms were positioned geometrically and constrained to ride on their parent atoms with C-H = 0.95-1.00 Å, and U_{iso} = 1.2−1.5 U_{eq} (parent atom). All calculations were performed using the SHELXL software and Olex2 graphical user interface.[22,23]

4BGIPN, CCDC number 2243340, $C_{60}H_{32}N_4$, Monoclinic, space group $P2_1$ (no. 4), a = 17.4217(4) Å, b = 15.2552(3) Å, c = 20.8314(6) Å, β = 114.583(3)°, V = 5034.6(2) Å^3, Z = 4, d_{calc} = 1.252 g cm^{-3}, μ = 0.623 mm^{-1}, yellow block, crystal size 33714 reflections measured

(4.664° ≤ 2Θ ≤ 152.79°), 17837 unique (R_{int} = 0.0314, R_{sigma} = 0.0512) which were used in all calculations. The final R_1 was 0.0462 (I > 2σ(I)) and wR_2 was 0.1190 (all data). *GOF* = 1.042, $\Delta\rho_{min}/\Delta\rho_{max}$ = 0.4/–0.2 e Å^{-3}.

Computational Results. Computations were performed using density functional theory (DFT) for the ground state and time-dependent DFT (TD-DFT) with Tamm-Dancoff approximation[24] for the excited states calculations, using the global hybrid MN15 functional by Truhlar[25] in combination with the def2-TZVP basis set by Ahlrichs.[26,27] TD-DFT calculations were performed to elucidate the nature of the excited state in a crystalline and optimized molecular geometry of **4BGIPN** with all data collected in the supporting information (Tables S1-S4). All calculations were carried out by Gaussian 16[28] and HOMO-LUMO overlap integrals were calculated using Multiwfn program.[29]

Supporting Information

Acknowledgment

We are grateful to ZEON EUROPE GmbH for providing ZEONEX® 480 Cyclo Olefin Polymer (COP) used in our studies.

Funding

This work was supported by the Royal Society and the Academy of Finland. A.S.R. acknowledges support from the Royal Society (grant nos. URF\R1\180288 and RGF\EA\181008). M.L. acknowledges the Academy of Finland Flagship Programme, Photonics Research and Innovation (PREIN), decision 320166. N.L.P. acknowledges the Doctoral Programme in Science, Technology and Computing (Sciteco, University of Eastern Finland). (TD)-DFT computations were made possible by use of the Finnish Grid and Cloud Infrastructure resources (urn:nbn:fi:research-infras-2016072533). AR acknowledges the support from the EPSRC (grant code EP/K039547/1).

References

[1] H. Uoyama, K. Goushi, K. Shizu, H. Nomura, C. Adachi, *Nature* **2012**, *492*, 234.

[2] A. Endo, M. Ogasawara, A. Takahashi, D. Yokoyama, Y. Kato, C. Adachi, *Adv. Mat.*, **2009**, *21*, 4802.

[3] C. A. Parker, C. G. Hatchard, *Trans. Faraday Soc.*, **1961**, *57*, 1894.

[4] Z. Yang, Z. Mao, Z. Xie, Y. Zhang, S. Liu, J. Zhao, J. Xu, Z. Chi, M. P. Aldred, *Recent advances in organic thermally activated delayed fluorescence materials*, Vol. 46, Royal Society of Chemistry, **2017**, pp. 915–1016.

[5] Y. Liu, C. Li, Z. Ren, S. Yan, M. R. Bryce, *All-organic thermally activated delayed fluorescence materials for organic light-emitting diodes*, Vol. 3, Nature Publishing Group, **2018**.

[6] M. A. Bryden, E. Zysman-Colman, *Organic thermally activated delayed fluorescence (TADF) compounds used in photocatalysis*, Vol. 50, Royal Society of Chemistry, **2021**, pp. 7587–7680.

[7] M. Y. Wong, E. Zysman-Colman, *Purely Organic Thermally Activated Delayed Fluorescence Materials for Organic Light-Emitting Diodes*, Vol. 29, Wiley-VCH Verlag, **2017**.

[8] Y. H. Lee, S. Park, J. Oh, J. W. Shin, J. Jung, S. Yoo, M. H. Lee, *ACS Appl. Mater. Interfaces.*, **2017**, *9(28)*, 24035.

[9] H. Kaji, H. Suzuki, T. Fukushima, K. Shizu, K. Suzuki, S. Kubo, T. Komino, H. Oiwa, F. Suzuki, A. Wakamiya, Y. Murata, C. Adachi, *Nat. Commun.*, **2015**, *6*, 8476.

[10] C. N. Muniz, J. Schaab, A. Razgoniaev, P. I. Djurovich, M. E. Thompson, *J. Am. Chem. Soc.*, **2022**, *144*, 17916.

[11] H. S. Kim, J. Y. Lee, S. Shin, W. Jeong, S. H. Lee, S. Kim, J. Lee, M. C. Suh, S. Yoo, *Adv. Funct. Mater.*, **2021**, *31*, 2104646.

[12] M. K. Etherington, N. A. Kukhta, H. F. Higginbotham, A. Danos, A. N. Bismillah, D. R. Graves, P. R. McGonigal, N. Haase, A. Morherr, A. S. Batsanov, C. Pflumm, V. Bhalla, M. R. Bryce, A. P. Monkman, *J. Phys. Chem. C*, **2019**, *123*, 11109.

[13] X.-K. Chen, Y. Tsuchiya, Y. Ishikawa, C. Zhong, C. Adachi and J.-L.Brédas, *Adv. Mater.*, **2017**, *29*, 1702767.

[14] M. A. Bryden, F. Millward, T. Matulaitis, D. Chen, M. Villa, A. Fermi, S. Cetin, P. Ceroni, E. Zysman-Colman, *J. Org. Chem.*, **2023**, *88(10)*, 6364.

[15] R. Ishimatsu, S. Matsunami, K. Shizu, C. Adachi, K. Nakano, T. Imato, *J. Phys. Chem. A*, **2013**, *117*, 5607.

[16] Gritzner, G.; Kůta, J., *Electrochim. Acta*, **1984**, *29*, 869.

[17] H. S. Kim, J. Y. Lee, S. Shin, Wo. Jeong, S. H. Lee, S. Kim, J. Lee, M. C. Suh, S. Yoo, *Adv. Funct. Mater.*, **2021**, *31*, 2104646

[18] M. K. Etherington, J. Gibson, H. F. Higginbotham, T. J. Penfold and A. P. Monkman, *Nature Commun*., **2016**, *7*, 13680.

[19] L.-S. Cui, A. J. Gillett, S.-F. Zhang, H. Ye, Y. Liu, X.-K. Chen, Z.-S. Lin, E. W. Evans, W. K. Myers, T. K. Ronson, H. Nakanotani, S. Reineke, J.-L. Bredas, C. Adachi and R. Friend, *Nat. Photon.*, **2020**, *14*, 636–642.

[20] P. L. dos Santos, J. S. Ward, D. G. Congrave, A. S. Batsanov, J. Eng, J. E. Stacey, T. J. Penfold, A. P. Monkman, M. R. Bryce, *Adv. Sci.*, **2018**, *5*, 1700989.

[21] Programs CrysAlisPro, Oxford Diffraction Ltd. Abingdon, UK, 2010.

[22] G. Sheldrick, Crystal structure refinement with SHELXL. *Acta Cryst. C* **2015,** *71* (1), 3-8.

[23] O. V. Dolomanov, L. J. Bourhis, R. J. Gildea, J. A. K. Howard, H. Puschmann, OLEX2: a complete structure solution, refinement and analysis program. *J. Appl. Cryst.* **2009,** *42* (2), 339.

[24] a) F. Furche, D. Rappoport, Density functional methods for excited states: equilibrium structure and electronic spectra. In: *Computational Photochemistry*; M. Olivuccim, Ed.; Elsevier: Amsterdam, **2005**, pp. 93–128; b) S. Hirata, M. Head-Gordon, *Chem. Phys. Lett.* **1999**, *314*, 291.

[25] Yu, H.S.; He, X.; Li, S.L.; Truhlar, D.G., *Chem. Sci*. **2016**, *7*, 5032.

[26] F. Weigend, M. Häser, H. Patzelt, R. Ahlrichs, *Chem. Phys. Lett.* **1998**, *294*, 143.

[27] F. Weigend, R. Ahlrichs, *Phys. Chem. Chem. Phys.* **2005**, *7*, 3297.

[29] M. J. Frisch, G. W. Trucks, H. B. Schlegel, G. E. Scuseria, M. A. Robb, J. R. Cheeseman, *Gaussian 16*, Revision A. 03; Gaussian Inc.: Wallingford CT, USA, 2016.

[29] T. Lu, F. Chen, *J. Comput. Chem.* **2012**, *33*, 580.